Selection of ν_μ Events for the MicroBooNE Deep Learning Low Energy Excess Analysis

The MicroBooNE Collaboration
October 29, 2018
MICROBOONE-NOTE-1051-PUB

1   Introduction

MicroBooNE is a large liquid argon time projection chamber (LArTPC) on Fermilab's Booster Neutrino Beam (BNB). A main goal of MicroBooNE is to search for the low energy excess (LEE) of electron like events seen by MiniBooNE. Using ν_μ interactions to constrain ν_e systematics is a common approach in oscillation experiments, we will adopt it here as well. This takes adantage of the high statistics ν_μ data and known correlations between electron and muon neutrino fluxes and cross sections. This note provides an overview of the selection of events with one reconstructed muon and one reconstructed proton in (μ1p) in MicroBooNE using a Deep Learning based reconstruction. We then present comparisons between data on our simulated neutrino interaction predictions for some important kinematic distributions. We find that in a sample of data corresponding to 4×10^{19} POT, that the data and simulation agree well in shape.

2   Overview of 1μ1p Selection

The selection is intended to isolate so called "1μ1p events". These events form our signal with which we will constrain the systematic uncertainties in a corresponding 1e1p selection of events. They are defined as any muon neutrino induced event which occurred inside a fiducial volume (defined by a rectangular prism 10 cm from the edge of the TPC active volume edges), remains fully contained, and yields one proton and one muon in the final state. Both particles must be energetic enough to produce clearly visible tracks, $E_\mu >$35 MeV and $E_p >$ 60 MeV. This topology is chosen because it provides strong handles to differentiate it from the cosmic background, while retaining efficiency for selecting low energy interactions. In the energy region for the expected signal, this class of events is predominantly predicted to be charged current quasi-elastic (CCQE) events. We will hereafter refer to events satisfying these criteria as "1μ1p signal."

For context, we provide an overview of the Deep Learning analysis, as shown in Fig. 1. MicroBooNE has an array of 32 PMTs that provide interaction information in parallel with the TPC. The analysis begins with a series of optical cuts designed to eliminate events with light patterns more consistent with only cosmic interactions than with neutrinos. The remaining stages make use of wire plane images. We use a set of cosmic tagging routines designed to identify charge associated with tracks that cross the active volume boundaries. Sets of untagged remaining charge are identified as contained regions of interest (cROIs) so long as they are matched to a reconstructed flash in the light collection system.

The subsequent step is the first that involves a deep learning algorithm, making use of a Semantic Segmentation Network (SSNet). This network treats each event like an image, and identifies if each pixel in that image is track like or shower like. These algorithms and techniques are described in detail separately[1][2]. These are the first application of such methods in LArTPC data analysis.

The next step is to identify and reconstruct vertices and associated tracks in 3D. Vertex seeds are first identified on each wire plane of the TPC by searching either for kinks in the intersection of two track segments or by searching for a shower cluster intersecting a track. If these seeds are consistent across multiple planes, a candidate vertex is generated.

The tracks and showers attached to each candidate vertex are then reconstructed in 3D via a stochastic search algorithm that identifies 3D consistent charge clusters emanating from the vertex. This 3D reconstruction provides the majority of the information that will be used in event selection: track lengths, angles, etc.
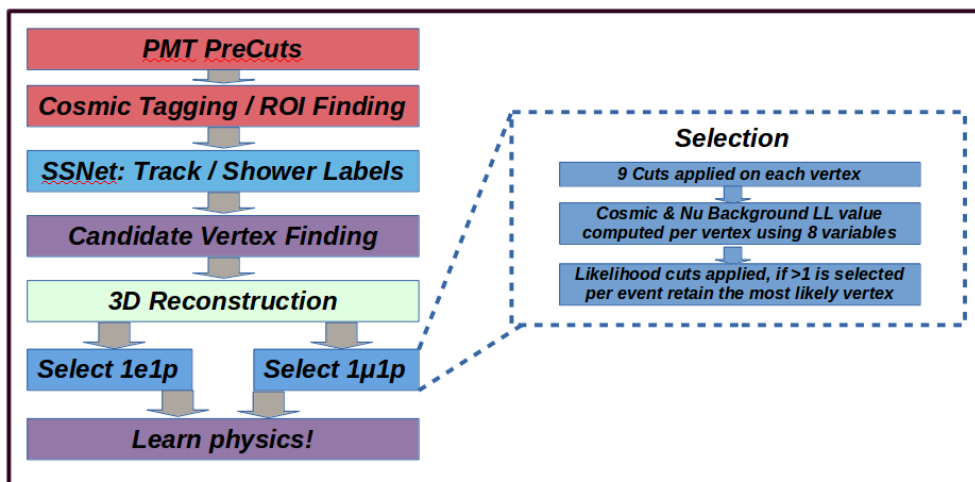

Figure 1: Overview of the deep-learning-based analysis chain.

3   Selection Procedure

Our signal 1μ1p is characterized by its one muon and one proton topology. Cosmic induced interactions in the TPC present our primary background. Secondary backgrounds come from neutrino interactions which do not satisfy our signal criteria (e.g. multiple protons, or tracks that exit the active volume).

We have developed the selection criteria using three samples: a sample of cosmic only data taken from periods of no beam to characterize and benchmark cosmic rejection; a simulated 1μ1p sample, and a simulated sample containing a full spectrum of interaction modes to characterize neutrino backgrounds. The simulated samples are overlaid with a sample of off beam cosmics. These samples have been filtered through the upstream segments of the chain, i.e. we are concerned, for instance, only with cosmic backgrounds that persist past

precut, cosmic tagging, and vertexing. To extract the $1\mu1p$ vertices from these backgrounds, we have developed the following selection criteria which a given vertex must satisfy.

3.1 Energy Reconstrution

Several of the selection methods we will discuss involve the reconstructed energy of the proton, muon, or neutrino. The energies deposited are obtained by using the known stopping power in LAr to convert track lengths to their initial energies. Deciding which track is the proton or muon is dictated by the average ionization of the tracks. The track with higher ionization is labeled the proton.

We also have three different ways to reconstruct the neutrino energy. Range based reconstruction uses the energy deposited by both tracks. CCQE based reconstruction uses only one particles based energy and the angle of that particle relative to the beam direction to estimate the energy assuming it is a pure CCQE interaction. This can be done for either the proton or the muon. We denote these $E_\nu^{range}, E_\nu^{QE-p}$, and $E_\nu^{QE-\mu}$ respectively. They are computed as follows

$$E_\nu^{QE-\mu} = \frac{1}{2} \frac{2(m_n - B)E_\mu - ((m_n - B)^2 + m_\mu^2 - m_p^2)}{(m_n - B) - E_\mu + p_\mu^z} \tag{1}$$

$$E_\nu^{QE-p} = \frac{1}{2} \frac{2(m_n - B)E_p - ((m_n - B)^2 + m_p^2 - m_\mu^2)}{(m_n - B) - E_p + p_p^z} \tag{2}$$

$$E_\nu^{range} = E_\mu + E_p + m_\mu + (m_n - m_p) + B \quad \text{where B} = 40 \text{ MeV}^1 \tag{3}$$

We will use these variables in the selection procedure that follows.

3.2 Initial Cuts

A given vertex must first satisfy the following cuts

1. The reconstructed vertex lies inside the fiducial volume.

2. Exactly two tracks are reconstructed.

3. The tracks show no evidence of faulty reconstruction - this is determined by the reconstruction algorithm's self diagnostic tools. [2]

4. Tracks must be fully contained in the active volume

---

[1] B accounts for the nuclear binding energy.

[2] The 3D reconstruction has several built in diagnostics intended to flag potential failures. These include, for example, methods to detect if a track that was being followed is becoming faint but does not abruptly stop.

5. We require consistency between three different initial neutrino energy reconstruction methods. We characterize the agreement between these reconstructed kinematics by defining the following three variables

$$\Delta_{p\mu} = E_\nu^{QE-p} - E_\nu^{QE-\mu} \tag{4}$$

$$\Delta_{\text{range}-\mu} = E_\nu^{QE-\mu} - E_\nu^{\text{range}} \tag{5}$$

$$\Delta_{\text{range}-p} = E_\nu^{QE-p} - E_\nu^{\text{range}} \tag{6}$$

In 3D, these form a cluster around 0 for signal, but are smeared out for various backgrounds. We require

$$\Delta_{p\mu}^2 + \Delta_{\text{range}-\mu}^2 + \Delta_{\text{range}-p}^2 < 1 \text{ GeV}^2$$

6. We make cuts on the reconstructed transverse momentum of the interaction. We define

$$p_T = |\vec{p}_\mu^{\,T} + \vec{p}_p^{\,T}| \tag{7}$$

$$\phi_T = cos^{-1}\left(\frac{\vec{p}_\mu^{\,T} \cdot \vec{p}_p^{\,T}}{p_\mu^T p_p^T}\right) \tag{8}$$

$$\alpha_T = cos^{-1}\left(\frac{\vec{p}_\mu^{\,T} \cdot \vec{p}_p^{\,T}}{p_\mu^T p^T}\right) \tag{9}$$

While all three will appear in the likelihood, only p_T and ϕ_T are cut. Specifically, we require

$$p_T < 500 MeV$$

$$\phi_T < \frac{3\pi}{8}$$

7. We require the reconstructed $Q^2 = 2E_\nu^{QE-p}(E_\mu - p_\mu cos(\theta_\mu)) - m_\mu^2$ to be greater than zero.

8. We finally reject events where the SSNet has identified significant shower activity in either one of the tracks. This helps remove muon bremsstrahlung, π^0 activity, and other shower like activity.

3.3 Likelihood Selection

Once we have the set of reconstructed tracks and vertices that pass the above cuts, we calculate variables which we will use to produce likelihood based discriminants to separate our signal from residual background. These are motivated by a mixture of known kinematics and shapes of ν_μ interactions and known common failure topologies. The variables used are:

1. η: the difference in reconstructed $\frac{dQ}{dx}$, normalized to sum of the reconstructed $\frac{dQ}{dx}$. This will be small for cosmics which have similar (MIP like) ionization on both tracks. This will be larger for a higher ionizing proton track attached to a minimum ionizing muon.

2. The 3D Opening angle between the tracks

3. The absolute difference in track ϕ, i.e. $|\phi_p - \phi_\mu|$

4. The sum of the track θ, i.e. $\theta_p + \theta_\mu$

5. p_T, as defined above

6. α_T, as defined above

7. ϕ_T, as defined above

8. Bjorken x, computed as $\frac{Q^2}{2M_p\nu}$, $\nu = E_\nu^{\text{range}} - E_\mu$

We produce probability distributions for cosmic vertices, signal vertices, and neutrino background vertices using the data and MC samples discussed above. We generate two sets of PDFs and correspondingly end up with two likelihood discriminants. One discriminates signal from cosmic vertices (Cosmic LL), the second discriminates signal from other neutrino induced background vertices (NuBkg LL). The final step in selection is a cut on both likelihood values at Cosmic LL > -3 and Neutrino Background LL (NuBkgLL) > 0

4 Data-MC Comparisons

Now that we have a selected set of $1\mu1$p events, we compare our prediction from simulation and cosmic background to our data.

We show kinematic variables which are ultimately derived from 9 measured quantities: 4 angles, 2 energies, and 3 positions. As a result some correlation between plots can be expected. These histograms are generated by running the full DL analysis and selection on a cosmic data sample and also on a simulation + cosmic data sample. This is used to generate a stacked prediction. The data is plotted overlaid. Here we are interested in the overall agreement in shape between the data and prediction, and so all distributions are then unit normalized.

The uncertainties shown are statistical. The uncertainty on the prediction is primarily driven by the cosmic contribution.
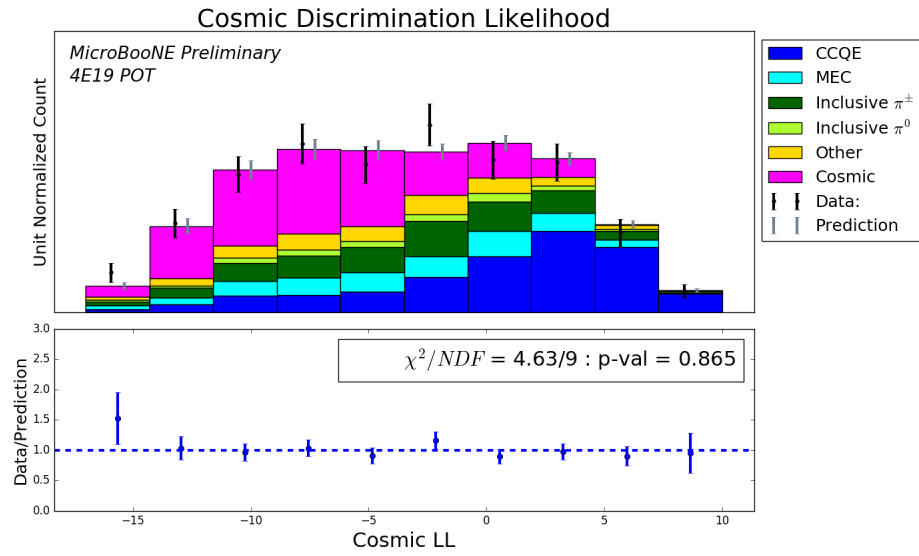
Figure 2: Cosmic discrimination likelihood, in the final selection $1\mu1$p events are selected with cosmic LL > -3.
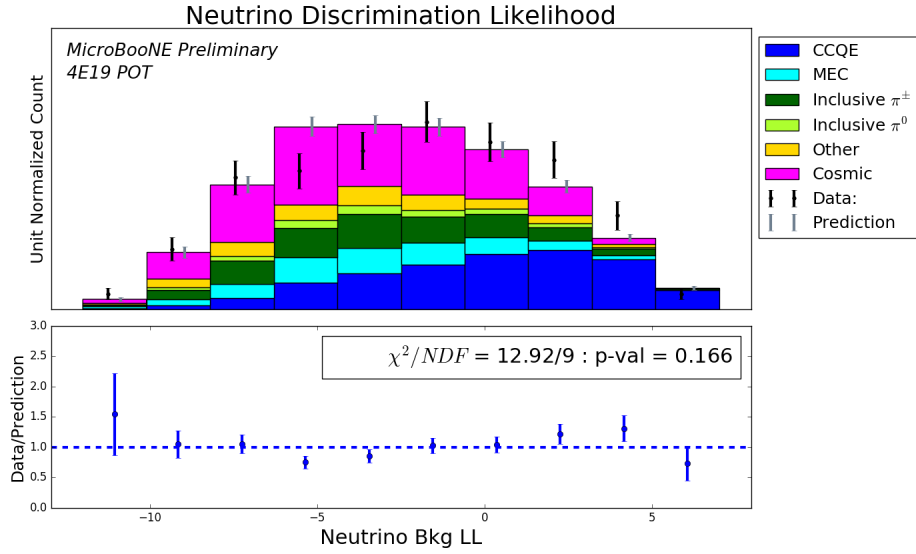
Figure 3: Neutrino background discrimination likelihood, in the final selection $1\mu1p$ events are selected with NuBkg LL > 0.
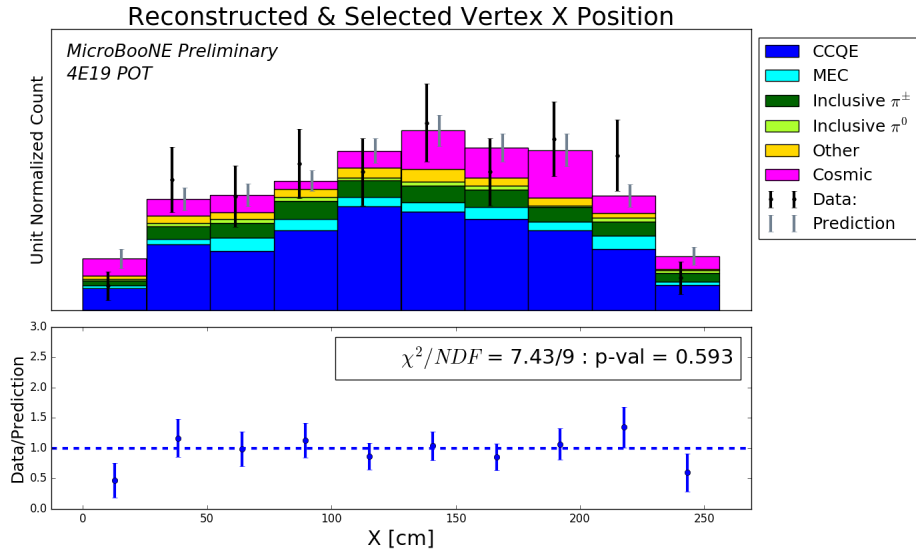

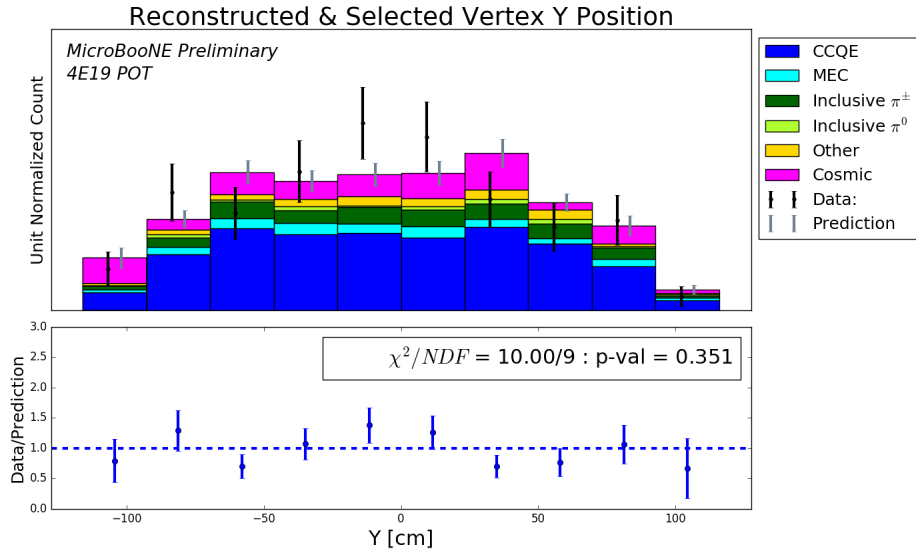Figure 4: Reconstructed neutrino vertex X position (drift direction).

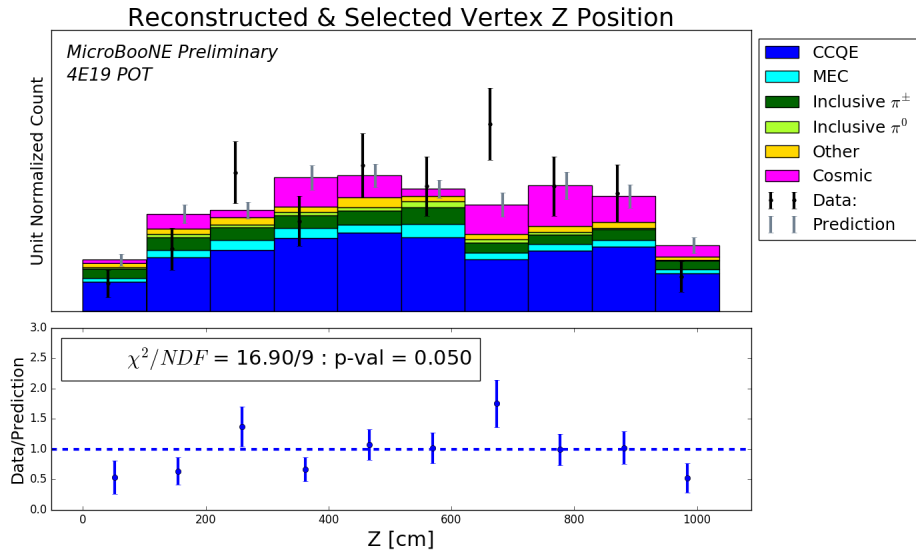Figure 5: Reconstructed neutrino vertex Y position (vertical direction).

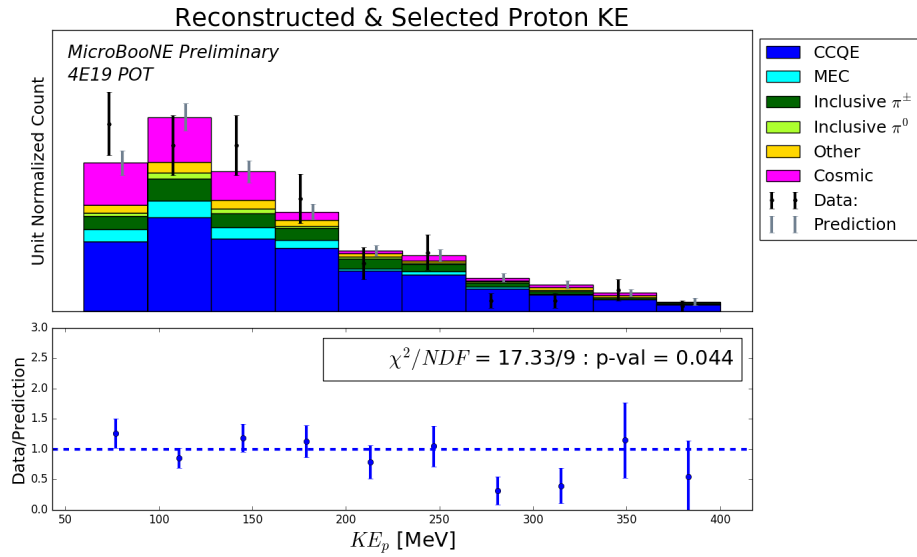Figure 6: Reconstructed neutrino vertex Z position (beam direction.)

Figure 7: Reconstructed proton kinetic energy, based on the track range.
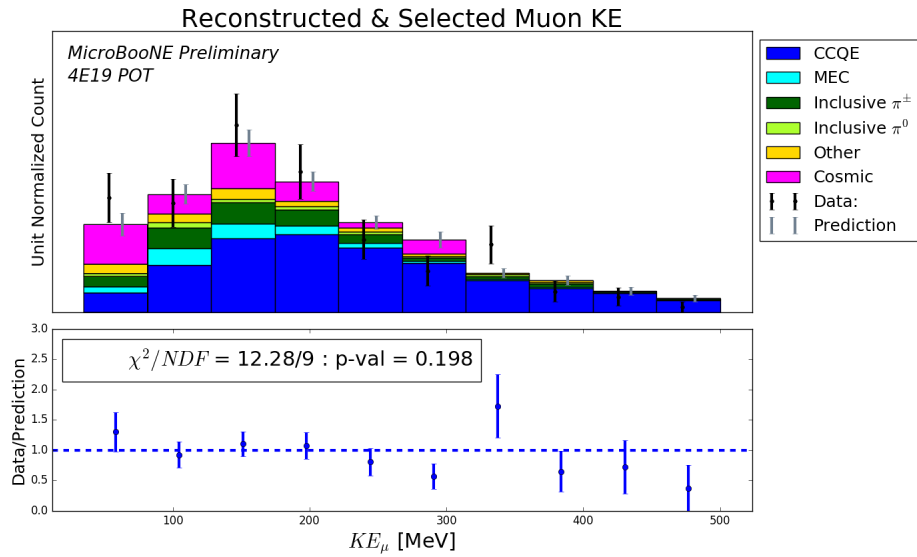
Figure 8: Reconstructed muon kinetic energy, based on the track range.

9
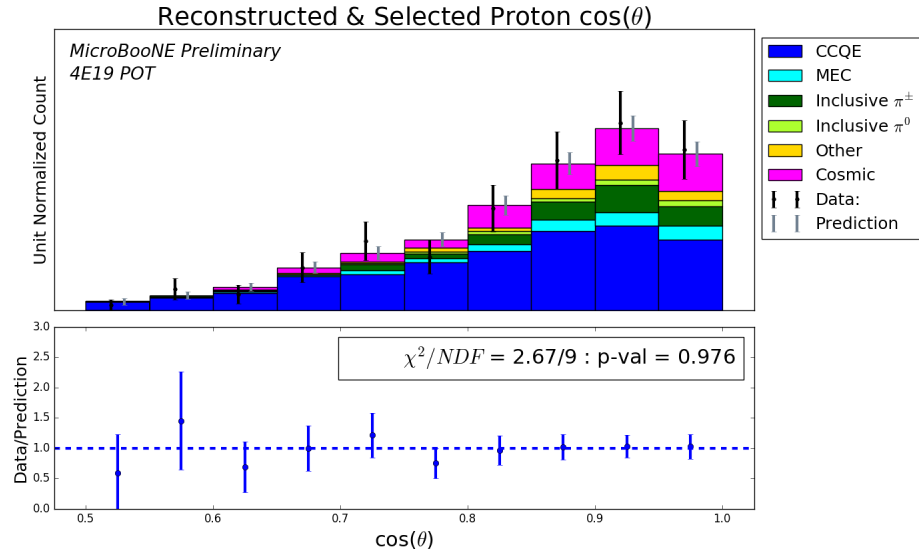
Figure 9: Reconstructed Proton $\cos(\theta)$, θ is the angle with respect to the beam.
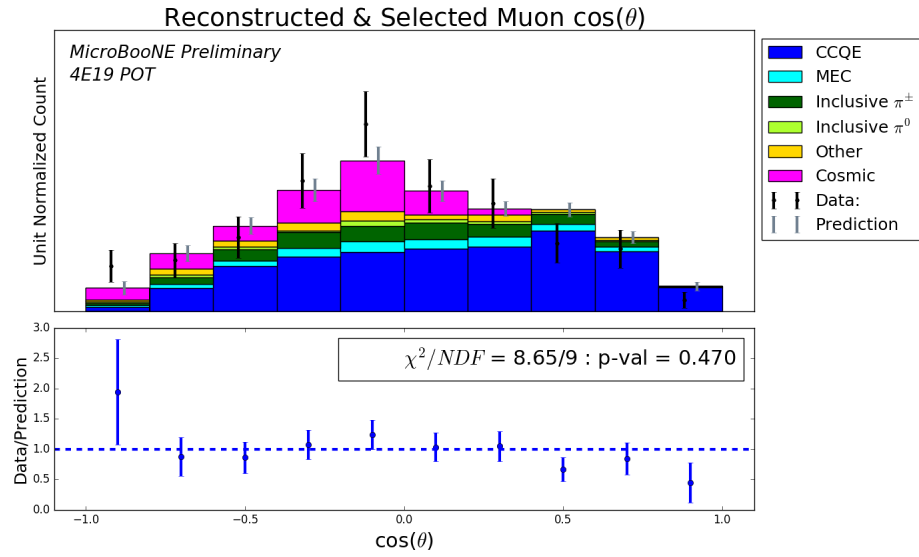
Figure 10: Reconstructed Muon $\cos(\theta)$, θ is the angle with respect to the beam.
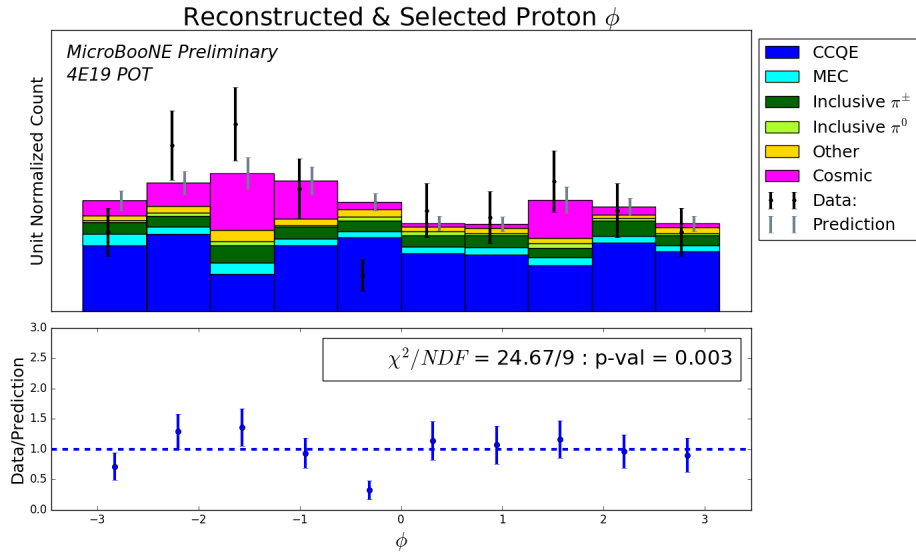
Figure 11: Reconstructed Proton ϕ. We note that there are known detector systematic effects which are not included in the uncertainties, but may contribute near $\phi \sim 0$
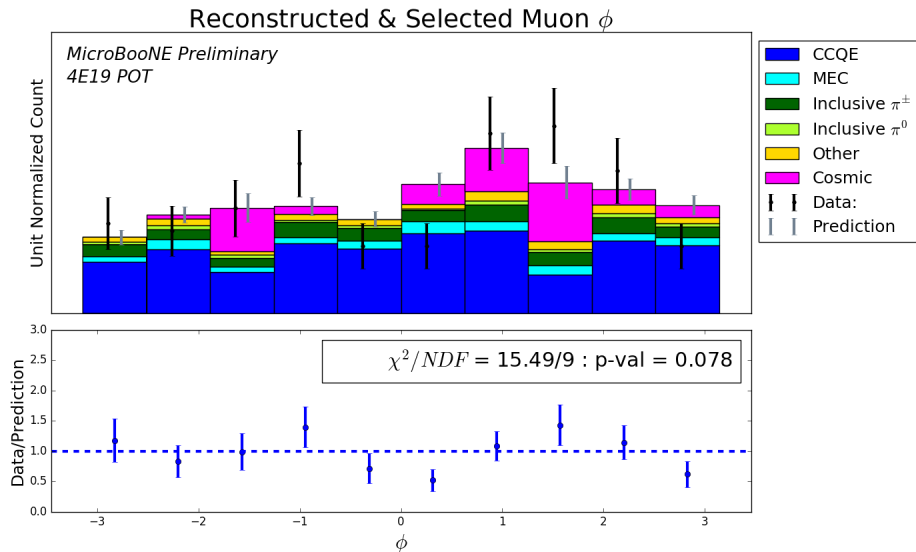
Figure 12: Reconstructed Muon ϕ.
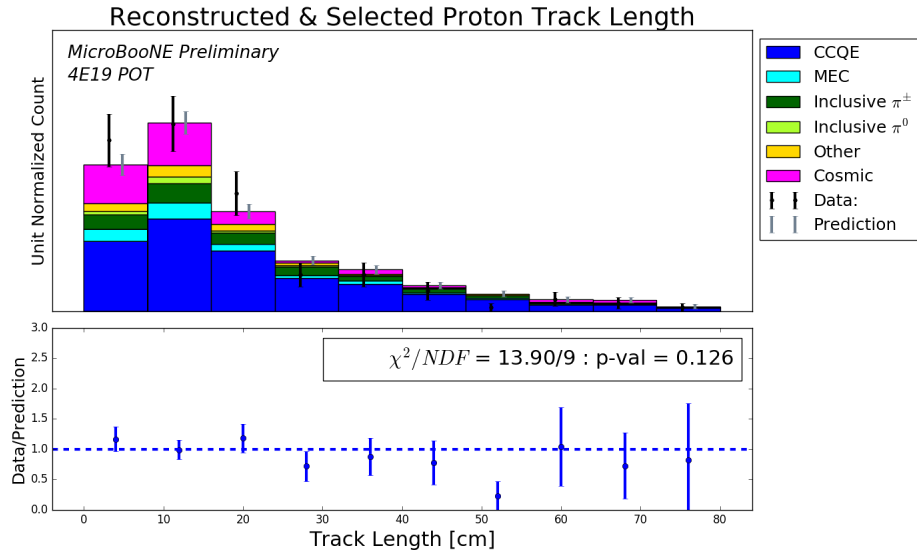
Figure 13: Reconstructed Proton Track Length.
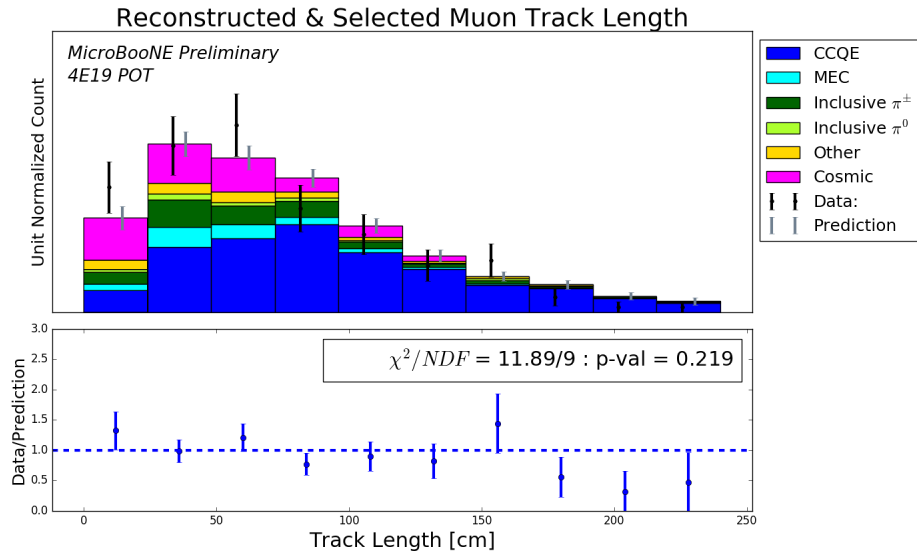
Figure 14: Reconstructed Muon Track Length.
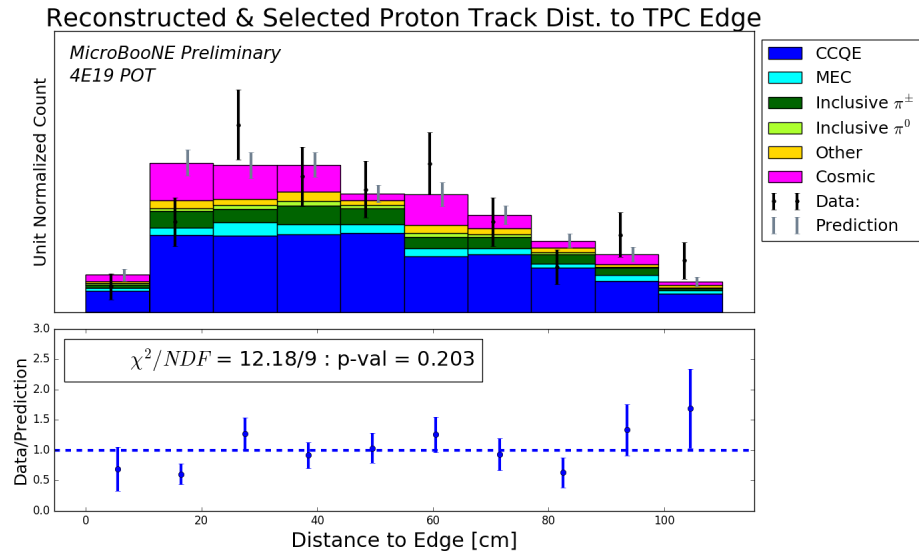
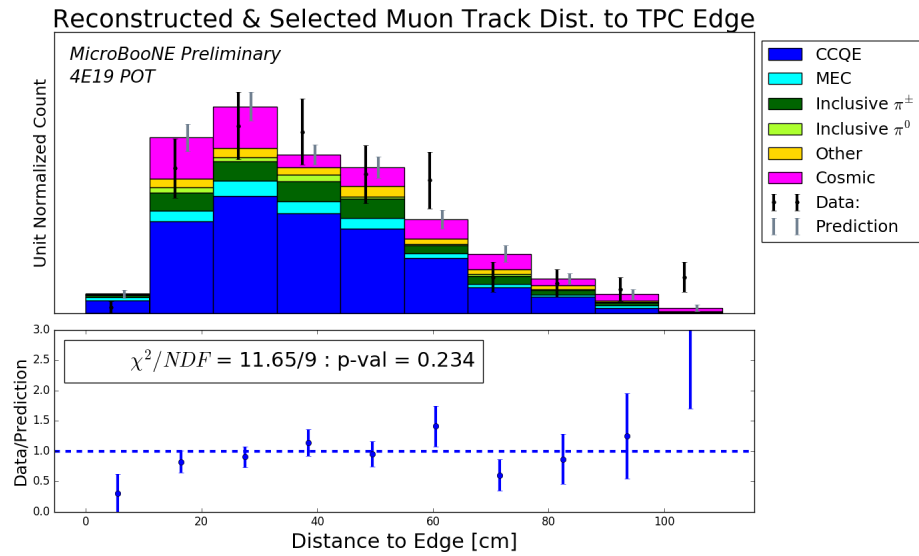Figure 15: Reconstructed Proton Track's Distance to Edge of Active TPC volume.

Figure 16: Reconstructed Muon Track's Distance to Edge of Active TPC volume. We note that there are systematic effects which are not included in the uncertainties which are known to have effects near the edge of the detector.
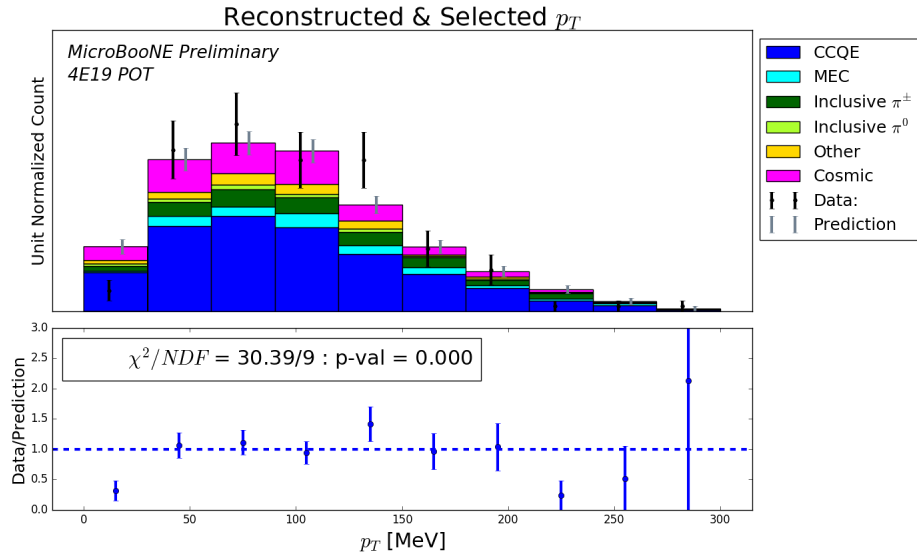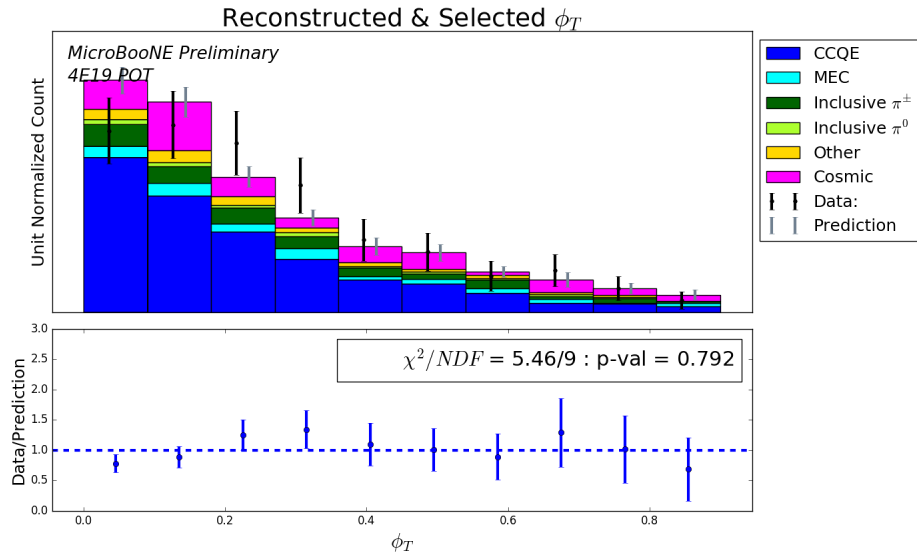
Figure 17: Reconstructed Transverse Variable p_T.

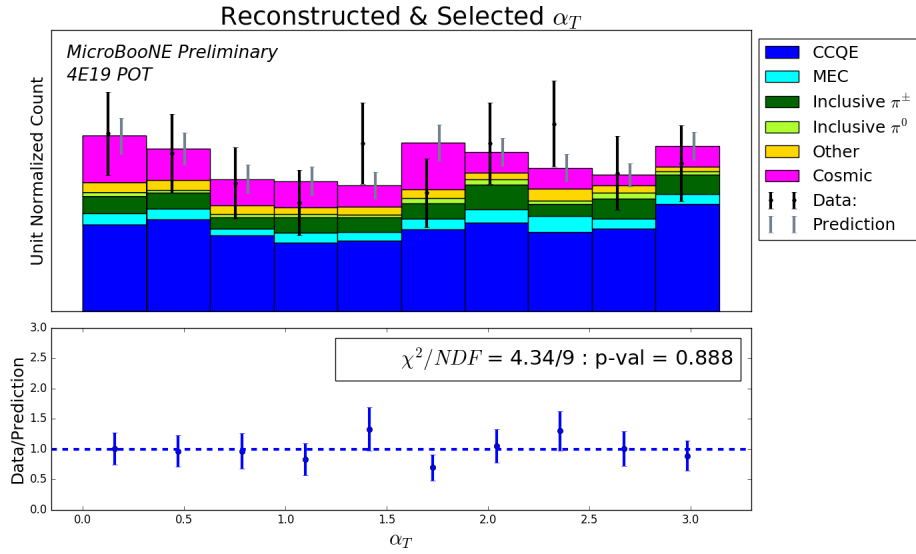Figure 18: Reconstructed Transverse Variable ϕ_T.

14

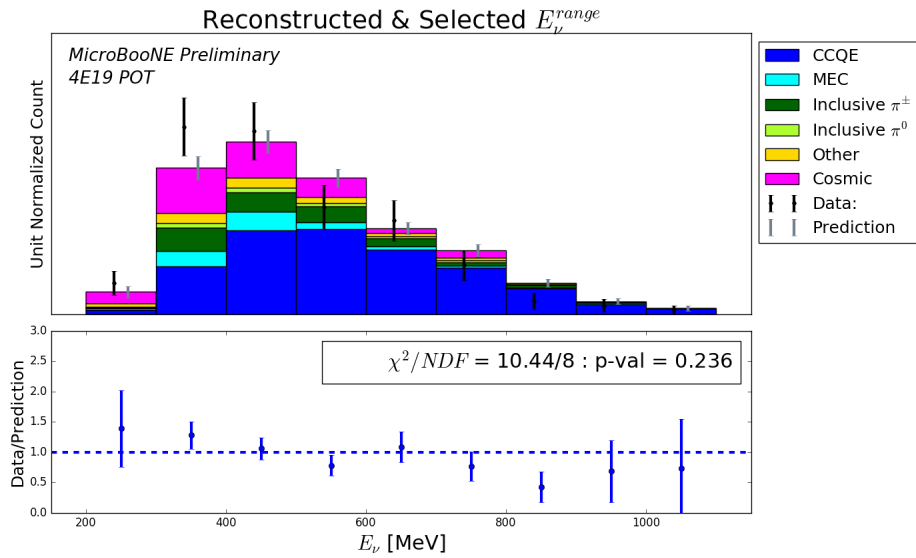Figure 19: Reconstructed Transverse Variable α_T.

Figure 20: Reconstructed neutrino energy E_ν^{range}. The ranged based energies for each particle, summing, and adding in binding energy and rest mass.
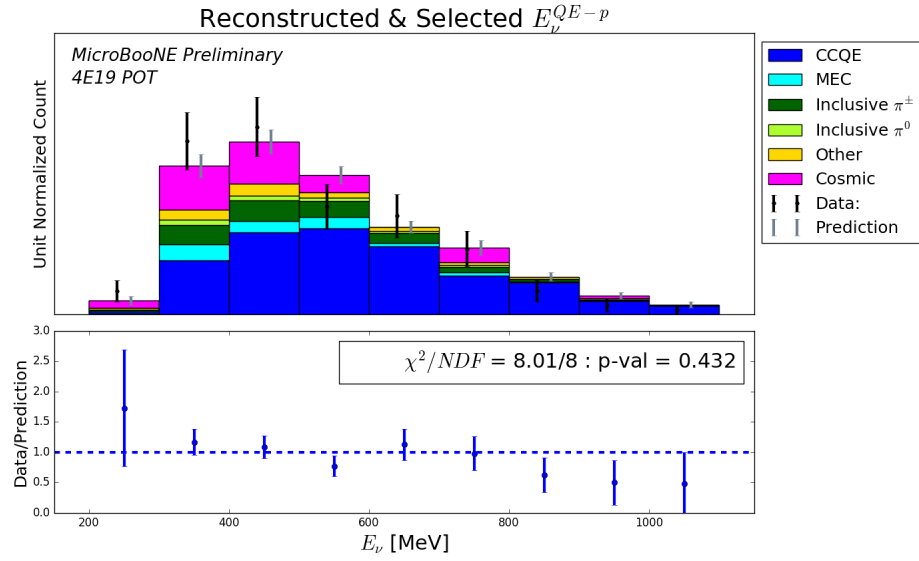
Figure 21: Reconstructed neutrino energy E_ν^{QE-p}. The energy from the QE reconstruction formula with the proton energy and angles.
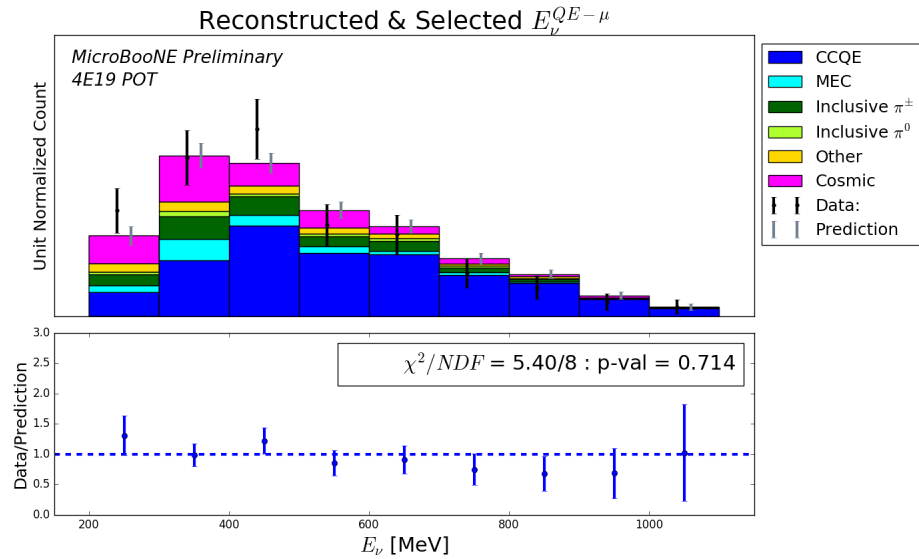

Figure 22: Reconstructed neutrino energy $E_\nu^{QE-\mu}$. The energy from the QE reconstruction formula with the muon energy and angles.
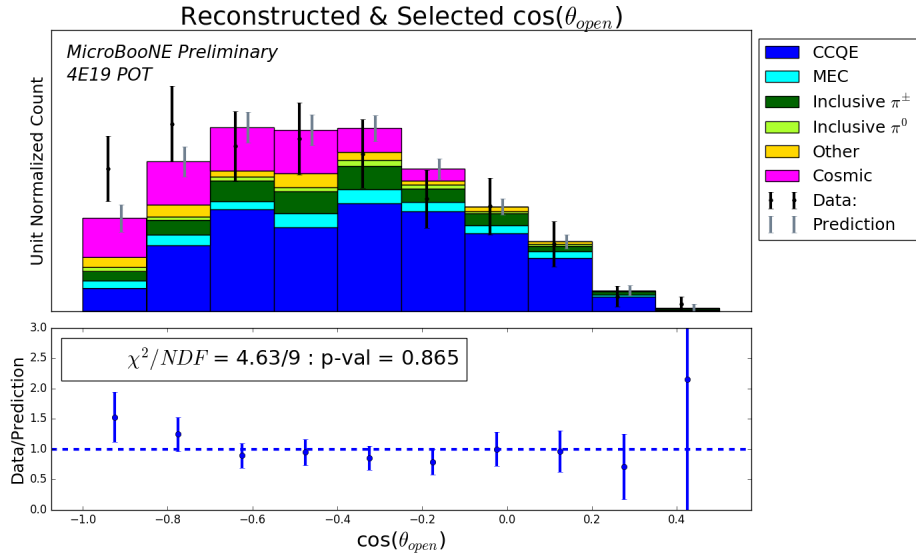
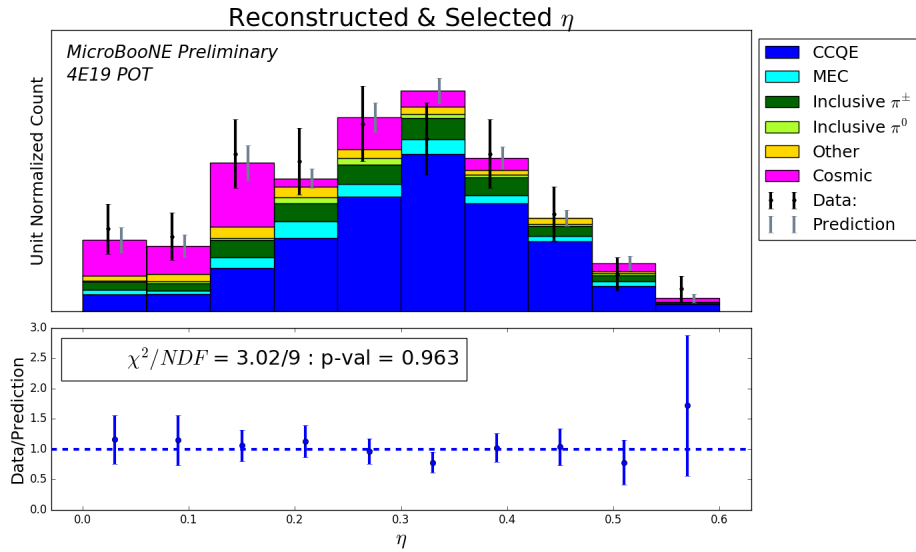Figure 23: Reconstructed two track opening angle.

Figure 24: Reconstructed η variable, which captures the ionization asymmetry between the two reconstructed tracks.

4.1 Conclusion

We summarize the variables and their χ^2 p-values below.

Variable	χ^2 **p-value**	Variable	χ^2 **p-value**
Cosmic LL	0.865	Proton Length	0.126
NuBkg LL	0.166	Muon Length	0.219
X Position	0.593	Proton Dist. to Edge	0.203
Y Position	0.351	Muon Dist. to Edge	0.234
Z Position	0.050	p_T	0.000
Proton KE	0.044	ϕ_T	0.792
Muon KE	0.198	α_T	0.888
Proton $\cos\theta$	0.976	E_ν^{range}	0.236
Muon $\cos\theta$	0.470	E_ν^{QE-p}	0.432
Proton ϕ	0.003	$E_\nu^{QE-\mu}$	0.714
Muon ϕ	0.078	η	0.963
$\cos\theta_{\mathrm{open}}$	0.865		

Table 1: Summary of χ^2 p-values for each histogram

Based on the χ^2 tests, there is good agreement between data and MC in the $1\mu1p$ sample. We observe a distribution of p-values consistent with a uniform distribution between 0.01 and 0.99 as we would anticipate under the hypothesis that the global agreement is good.

Our results indicate that the deep learning analysis is reaching sufficient maturity to begin to implement it as the constraint on signal systematics for the low energy excess analysis.

4.2   References

[1] A Deep Neural Network for Pixel-Level Electromagnetic Particle Identification in the MicroBooNE Liquid Argon Time Projection Chamber MicroBooNE Collaboration arXiv:1808.07269, submitted to PRD

[2] Convolutional Neural Networks Applied to Neutrino Events in a Liquid Argon Time Projection Chamber - MicroBooNE Collaboration JINST 12 (2017) no.03, P03011 arXiv:1611.05531